Transient simulation of a pneumatic sharp edged L-shaped pipe

REVIEWED

Filipp Kratschun, Joscha Enking and Hubertus Murrenhoff

RWTH Aachen University, Institute for Fluid Power Drives and Systems (IFAS),
Campus Boulevard 30, D-52074 Aachen, Germany
E-Mail: filipp.kratschun@ifas.rwth-aachen.de

The increase of system dynamic within the area of pneumatics requires sophisticated numerical methods to determine the systems' performance. Cycle durations in the range of just a few milliseconds and below require the implementation of transient gas dynamic solvers to predict the systems behavior accurately and to save computational time. Yet, such solvers lack of accuracy for sharp edged elbows. This paper presents a hybrid approach using a one dimensional and a two dimensional finite volume Riemann-Solver. The results are compared to analytical acoustics theory and to a CFD approach using a turbulence model.

Keywords: System Simulation, Pneumatics, Numerical Solver, Gasdynamics
Target audience: Automation, Pneumatic Systems, Simulation

1 Introduction

In general, it is possible to calculate several flow parameters for transient pneumatic flows using computational fluid dynamics (CFD) software including turbulence modelling for instance for a highly dynamic automation application or a gaseous fuel injection system. Despite increasing processing power of modern computers solving particular problems is yet time-consuming. A simulation of a few milliseconds results in a computational time of several hours which makes the design of a highly dynamic pneumatic system resource consuming. Therefore, one dimensional numerical solvers based on Euler Equations are commonly used to achieve reasonably short simulation duration and yet retaining sufficient accuracy. However, such solvers are not capable of simulating the entire spectrum of flow regimes and geometries which occur in pneumatic components like sharp edged elbow fittings. The flow regime of a miter joint lies within a full reflection and transimission of the incoming mass flow and pressure waves. A one dimensional solver can only offer one of the two regimes, either full reflection or full transmission. Accordingly, a solution of a partially transmitted and partially reflected wave is not possible to compute. This paper presents an approach to simulate a sharp edged elbow using a two dimensional solver within the inner part of the joint which is coupled to one dimensional solver at the outer parts. Both solvers are based on the Flux Vector Splitting (FVS) approach presented by Steger and Warming /1/. This approach allows the calculation of a partial transmission and partial reflection of a miter joint time efficiently. The results are compared to acoustic theory and CFD solution in order to validate the solver.

2 Governing equations and numerical approach

To describe one dimensional gaseous flows Euler Equations are commonly used since for large Reynolds numbers viscosity influence can be neglected. These include the continuity equation, momentum and energy equation and are given by Equation (1). Herein, e is the specific energy described by Equation (2).

$$\frac{\partial}{\partial t}\begin{pmatrix}\rho\\ \rho u\\ e\end{pmatrix}+\frac{\partial}{\partial x}\begin{pmatrix}\rho u\\ \rho u^2+p\\ u(e+p)\end{pmatrix}=0 \tag{1}$$

$$e=\rho c_v T+\rho u^2 \tag{2}$$

For a perfect gas the isochoric heat capacity c_v can be expressed via Equation (3) using the specific gas constant R and the heat capacity ratio κ of the given gas. Subsequently, the specific energy of the system can be described using pressure, density and velocity only, leading to Equation (4).

$$c_v=\frac{R}{\kappa-1} \tag{3}$$

$$e=\frac{p}{\kappa-1}+\rho u^2 \tag{4}$$

This results in a decoupled system given by Equation (5) which consists of conservative variables U. Herein, the function $F(U)$ is the flux function of the mass, energy and momentum flux. The conservative variables U_i can be expressed via primitive variables ρ, u and p applying Equation (6) /1/.

$$U_t+F(U)_x=0 \tag{5}$$

$$U_1=\rho,\qquad U_2=\rho u,\qquad U_3=\frac{p}{\kappa-1}+\rho u^2 \tag{6}$$

To allow the occurrence of shocks and other discontinuities which, for instance, can be caused during the opening process of a valve it is necessary to use the conservative formulation of Eulerian Equations. If the time integration is done numerically and the computational domain is discretised (figure 1 a) the numerical scheme is given by Equation (7). Herein, i is the local index of a cell and n is the index of the current time step.

$$\widetilde{U}_i^{n+1}=\widetilde{U}_i^n-\frac{\Delta t}{\Delta x}\left(F\left(\widetilde{U}\right)_{i+\frac{1}{2}}^n-F\left(\widetilde{U}\right)_{i-\frac{1}{2}}^n\right) \tag{7}$$

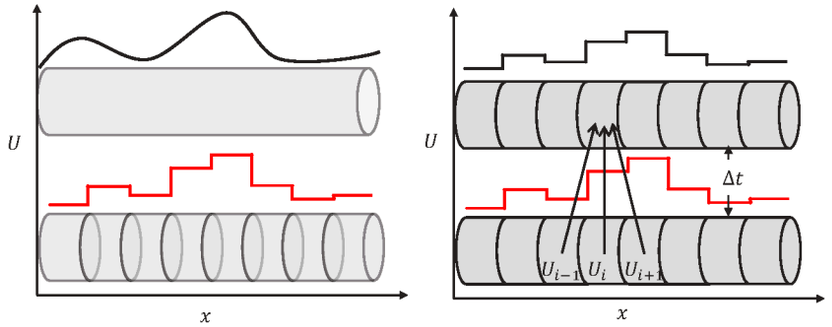

Figure 1: Finite volume and explicit solver.

The flux values of the inter cell fluxes $F\left(\widetilde{U}\right)_{i+\frac{1}{2}}^n$ and $F\left(\widetilde{U}\right)_{i-\frac{1}{2}}^n$ are calculated using the current averaged cell value i and its neighbours i-1 and i+1, which is illustrated in figure 1b. The flux formulation is chosen the way it is proposed by Steger and Warming /1/. This scheme utilises the hyperbolic character of Equation (1), which means that it possesses defined propagation speeds of information, namely the eigenvalues $\lambda_1=u-a$, $\lambda_2=u$ and $\lambda_3=u+a$. Herein, a is the speed of sound and can be calculated for a perfect gas applying Equation (8). For a more detailed description of hyperbolic systems and its properties the reader is referred to /2/.

$$a=\sqrt{\kappa\frac{p}{\rho}} \tag{8}$$

Steger and Warming construct a numerical inter cell flux which depends on the eigenvalues λ_i of the system and can therefore be given a defined propagation achieving a separation of positive and negative flux components described by Equation (9) wherein H is described by Equation (10).

$$F_i^{\pm} = \frac{\rho_i}{2\kappa}\begin{pmatrix} \lambda_1^{\pm} + 2(\kappa-1)\lambda_2^{\pm} + \lambda_3^{\pm} \\ (u-a)\lambda_1^{\pm} + 2(\kappa-1)u\lambda_2^{\pm} + (u+a)\lambda_3^{\pm} \\ (H-ua)\lambda_1^{\pm} + (\kappa-1)u^2\lambda_2^{\pm} + (H+ua)\lambda_3^{\pm} \end{pmatrix} \tag{9}$$

$$H = \frac{1}{2}u^2 + \frac{a^2}{\kappa-1} \tag{10}$$

The incoming flux $F(\tilde{U})^n_{i-\frac{1}{2}}$ at the left cell interface is composed of the positive part of the left cell's flux and the negative component of the current cell, see figure 2 a,b. The outgoing flux $F(\tilde{U})^n_{i+\frac{1}{2}}$ is built with the positive flux component of the current cell and the negative component of the right cell.

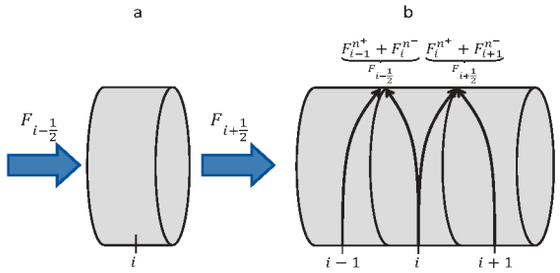

Figure 2: Numerical Flux by Steger Warming.

Finally the entire numerical scheme can be summarised in Equation (11). To verify its accuracy for small disturbances the acoustic theory for a closed and opened resonator is applied. The modulation of boundary conditions for a closed and an open end for a finite volume solver is taken from /2/ and /3/.

$$\tilde{U}_i^{n+1} = \tilde{U}_i^n - \frac{\Delta t}{\Delta x}\left(F_i^{n^+} + F_{i+1}^{n^-} - F_{i-1}^{n^+} - F_i^{n^-}\right) \tag{11}$$

2.1 1-D Solver validity for small disturbances

To demonstrate the validity of the solver a pipe with the length L and an open end is excited by a sinusoidal pressure signal at the very first cell. The frequency is chosen to be the second order harmonic oscillation $f_{\text{open},2}$ Equation (12) /4/. If the solver does represent the physics correctly, three nodes and two anti-nodes should occur along the tube's length. The first node has to be at the very beginning of the pipe, the second one has to be exactly in the middle of the pipe and the third one is to be expected at the end of the pipe. Whereas two anti-nodes have to be exactly in between the nodes.

$$f_2 = \frac{a}{L} \tag{12}$$

Figure 3 shows the pressure distribution over time and space in a pipe of the length $L = 0.2\ m$. To assure the validity of the acoustic theory the pressure disturbance is chosen to be very small (0.1 bar) compared to the mean pressure which is 10 bar. It can clearly be seen, that as predicted by the theory there are exactly three nodes at the beginning, in the middle and at the end of the pipe. In between the two anti-nodes are located.

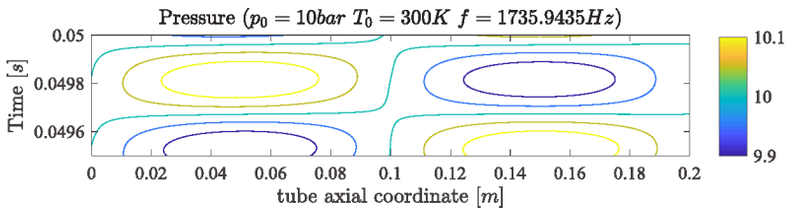

Figure 3: Open end resonator test

Furthermore a second order oscillation for a closed end is examined (figure 4), whose frequency is given by Equation (13) /5/.

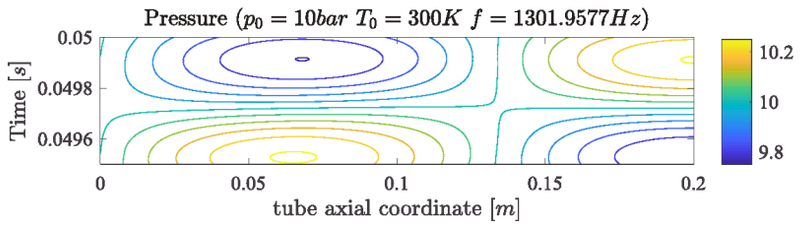

Figure 4: Closed end resonator test

In this case, two nodes and two antinodes are expected. The second anti-node should be exactly in the end of the pipe, whereas the first one has to lie on one third of the entire tube's length. The first node is to be expected at the entering and the second one at two thirds of the tube's length.

$$f_2 = \frac{3a}{4L} \tag{13}$$

As expected, the solver calculates the position of the nodes and anti-nodes as predicted by the acoustic theory. To demonstrate the impact of a sharp edged elbow on the harmonic oscillation a 2-D solver is introduced in the following section.

3 Implementation of the 2-D solver

This chapter deals with the implementation of the two dimensional scheme and its coupling to the one dimensional solver in for an elbow. The solver is tested in conjunction with the acoustic theory for a closed end and an open end resonator.

3.1 Governing numerical scheme

To produce a partial reflection numerically within an elbow it is necessary to implement a two dimensional solver within the inner part of it. As presented before, the finite volume solver by Steger and Warming is taken into account for the two dimensional case as well. The increase of one dimension implies an additional momentum equation and flux G, yet the principle of the solver remains the same and is depicted in figure 5.

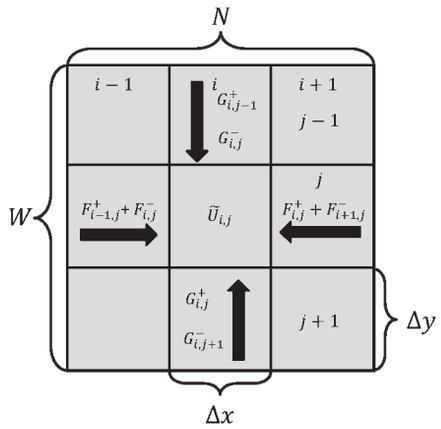

Figure 5: 2-D-scheme.

The numerical scheme for the solver is the same as for the one dimensional solver and if the local discretisation in x-direction is of the same size as for the y-direction the numerical scheme is presented in Equation (14).

$$\tilde{U}_i^{n+1} = \tilde{U}_i^n - \frac{\Delta t}{\Delta x}\left(F_{i,j}^{n^+} + F_{i+1,j}^{n^-} - F_{i-1,j}^{n^+} - F_{i,j}^{n^-}\right) - \frac{\Delta t}{\Delta y}\left(G_{i,j}^{n^+} + G_{i,j+1}^{n^-} - G_{i,j-1}^{n^+} - G_{i,j}^{n^-}\right) \tag{14}$$

The numerical flux calculation requires the knowledge of the eigenvalues, i.e. the characteristic speeds. In the case of a two dimensional problem there are eight of them in total (four for each direction) instead of three for the one dimensional case. For the x-direction the first one is $\lambda_1 = u - a$, the fourth one is $\lambda_4 = u + a$ and the second and third are identical $\lambda_2 = \lambda_3 = u$. Hence, to calculate the fluxes in x-direction for each cell Equation (15) is applied.

$$F_{i,j} = \frac{\rho_{i,j}}{2\kappa}\begin{pmatrix} \lambda_1^{\pm} + 2(\kappa-1)\lambda_2^{\pm} + \lambda_4^{\pm} \\ (u-a)\lambda_1^{\pm} + 2(\kappa-1)u\lambda_2^{\pm} + (u+a)\lambda_4^{\pm} \\ \lambda_1^{\pm} v + 2(\kappa-1)\lambda_2^{\pm} v + \lambda_4^{\pm} v \\ (K-ua)\lambda_1^{\pm} + (\kappa-1)(u^2+v^2)\lambda_2^{\pm} + (K+ua)\lambda_4^{\pm} \end{pmatrix} \tag{15}$$

The eigenvalues ξ for the y-direction are calculated the same way as for the x-direction but instead of using the horizontal velocity u the vertical velocity v is applied leading to $\xi_1 = v - a$, $\xi_4 = v + a$ and $\xi_2 = \xi_3 = v$. Finally the numerical flux in y-direction is constructed in Equation (16).

$$G = \frac{\rho_{i,j}}{2\kappa}\begin{pmatrix} \xi_1^{\pm} + 2(\kappa-1)\xi_2^{\pm} + \xi_4^{\pm} \\ \xi_1^{\pm} u + 2(\kappa-1)\xi_2^{\pm} u + \xi_4^{\pm} u \\ (v-a)\xi_1^{\pm} + 2(\kappa-1)v\xi_2^{\pm} + (v+a)\xi_4^{\pm} \\ (K-va)\xi_1^{\pm} + (\kappa-1)(u^2+v^2)\xi_2^{\pm} + (K+va)\xi_4^{\pm} \end{pmatrix} \tag{16}$$

Since the additional velocity component v does not only contribute to an additional momentum but also to an additional kinetic energy, the energy flux has to consider that component which results in Equation (17) which is different to that of Equation (10) for the one dimensional case.

$$K = \frac{1}{2}(u^2 + v^2) + \frac{a^2}{\kappa - 1} \tag{17}$$

Having defined the numerical fluxes for the two dimensional system, it is now possible to compute an elbow using the two dimensional solver only but obviously the computational time would increase by the power of two. To overcome that problem only the inner part of the elbow is calculated using the two dimensional scheme, which is depicted in figure 6. Here, the upper part is divided into a region with length L_{1D} where the one dimensional solver is applied and a two dimensional region L_{2D} connecting the adjacent ones. The computational effort is reduced thereby but the border between the regions needs special mathematical treatment.

Regarding Equation (11) the one dimensional cell at the border requires a neighbour cell of equivalent size to calculate the inter cell fluxes. Since the next neighbour cell belongs to the two dimensional solver the necessity of an averaging method arises. One could simply use an averaging of the primitive variables p, ρ, u and v for the two dimensional cells but that would result in momentum and energy annihilation. This is caused by the fact that for the vertical one dimensional solver the horizontal velocity components of the two dimensional solver would be neglected. For the horizontal one dimensional border cell the same problem occurs for the vertical velocity components of the two dimensional solver, meaning that all vertical velocity components would disappear since they cannot be included into the one dimensional scheme.

Therefore, another approach is presented which prevents the annihilation. Instead of averaging the primitive variables an averaging of the conservative variables is presented and retransformed to the primitive variables using Equation (5) which is discussed more detailed in the following.

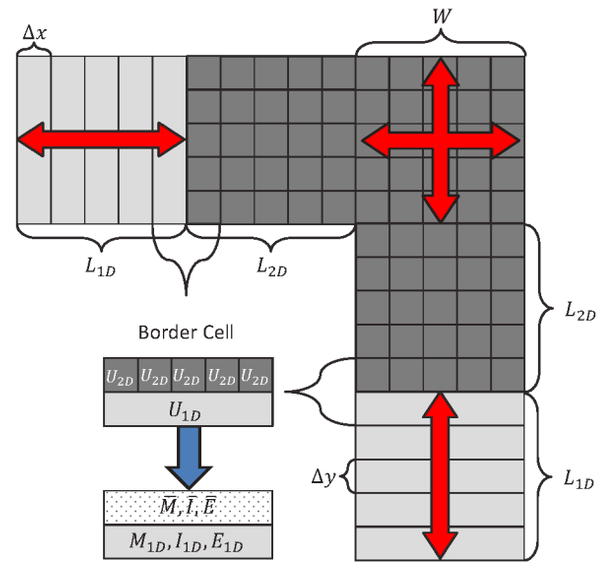

Figure 6: 2-D-scheme for elbow discretisation

3.2 Coupling of 1- and 2-dimensional solver

Firstly, the border cell of the horizontal one dimensional solver (border of L_{2D} and L_{1D} in the upper part of the elbow) is treated. Regarding figure 6 the elbow's width is described by W. The total amount of cells in vertical direction within the two dimensional part of the solver is therefore V and can be calculated by the trivial Equation (18).

$$V = \frac{W}{\Delta y} \tag{18}$$

The total averaged mass $M_{2D,vert}$ of the two dimensional cells at the border is, therefore, the sum of all cell masses in y-direction given by Equation (19).

$$M_{2D,\mathrm{vert}} = \sum_{j=1}^{j=V} \rho_{i,j}\, \Delta x \Delta y \tag{19}$$

To guarantee mass conservation this mass has to be exactly the same as the mass of a one dimensional cell with the width W, the length Δx and the averaged density $\bar{\rho}$ which is given by Equation (20). Equalising (19) with (20) leads to Equation (21) to calculate the averaged density for the two dimensional cells.

$$\bar{M} = \bar{\rho}_{\mathrm{vert}} \Delta x W \tag{20}$$

$$\bar{\rho}_{\mathrm{vert}} = \sum_{j=1}^{j=V} \rho_{i,j} \frac{\Delta y}{W} \tag{21}$$

For the momentum conversion two contributions have to be considered, the horizontal one (22) and the vertical one (23).

$$I_{2D,\mathrm{vert,x}} = \sum_{j=1}^{j=V} \rho_{i,j} u_{i,j}\, \Delta x \Delta y \tag{22}$$

$$I_{2D,\mathrm{vert},y} = \sum_{j=1}^{j=V} \rho_{i,j} v_{i,j}\, \Delta x \Delta y \tag{23}$$

The sum of the momentum contributions $I_{2D,vert,x}$ and $I_{2D,vert,y}$ have to be exactly the momentum of an averaged cell with the length Δx, the width W and averaged momentum $\bar{\rho}\bar{u}$ given by Equation (24). Equalizing the sum of (22) and (23) with (24) leads to Equation (25), which is the averaged velocity in x-direction of the two dimensional solver.

$$\bar{I} = \bar{\rho}\bar{u}\Delta x W \tag{24}$$

$$\bar{u}_{\mathrm{vert}} = \frac{1}{\bar{\rho}_{\mathrm{vert}}} \left(\left| \sum_{j=1}^{j=V} \rho_{i,j} v_{i,j} \right| + \sum_{j=1}^{j=V} \rho_{i,j} u_{i,j} \right) \frac{\Delta y}{W} \tag{25}$$

In order to obtain an averaged pressure for the two dimensional border region firstly the total energy given by Equation (26) is calculated and the averaged pressure $\bar{p}_{\mathrm{vert}}$ is extracted from it subsequently since the averaged velocity and density are known by now.

$$\bar{E}_{\mathrm{vert}} = \left(\frac{\bar{p}}{\kappa - 1} + \frac{1}{2} \bar{\rho} \bar{u}^2 \right) \Delta x W \tag{26}$$

The total amount of energy of the two dimensional cells along in the y-direction has to be calculated invoking Equation (27) which contains the vertical and the horizontal velocity components. The conservation of energy requires the equality of Equation (26) and (27) which results in Equation (28), giving an expression for an averaged pressure $\bar{p}_{\mathrm{vert}}$.

$$E_{2D,\mathrm{vert}} = \sum_{j=1}^{j=V} \left(\frac{p_{i,j}}{\kappa - 1} + \frac{\rho_{i,j}}{2} \left(u_{i,j}^2 + v_{i,j}^2 \right) \right) \Delta x \Delta y \tag{27}$$

$$\bar{p}_{\mathrm{vert}} = \left(\sum_{j=1}^{j=V} \left(\frac{p_{i,j}}{\kappa - 1} + \frac{\rho_{i,j}}{2} \left(u_{i,j}^2 + v_{i,j}^2 \right) \right) \frac{\Delta y}{W} - \frac{1}{2} \bar{\rho} \bar{v}^2 \right) (\kappa - 1) \tag{28}$$

All primitive variables for the border region of the horizontal part of the elbow have been obtained avoiding momentum or energy annihilation. For the lower part i.e. for the averaging in x-direction the procedure is straight forward and will not be explained in detail here.

3.3 Numerical results using 2-D solver

A sharp elbow is examined in terms of the acoustic theory in this section. The horizontal pipe has the same length $L = 0.1\ m$ as the vertical pipe. To validate the behaviour of the 2-D solver two cases, an open elbow and a semi closed elbow are presented.

The coupled 1-D solver is used for the front and back end of the elbow with the length of $L_{1D} = 0.075m$. To reveal streamline curvature behind the elbow the 2-D solver is not only used for the actual corner but also for a region before and behind the corner with a length $0.05m$.

Figures 7 and 8 show that no discontinuity at $x = 0.075m$ and $x = 0.125m$ is caused by the averaging method. Therefore, the mathematical coupling as described in section 3.2 results in an accurate numerical solution without causing numerical oscillation which would lead to artificial numerical pressure waves disturbing the pattern predicted by the acoustic theory.

In comparison to the acoustic behaviour of the sharp elbow to the straight pipe, the first cell is excited by the same sinusoidal pressure input as in section 2.1. With the second order harmonic oscillation $f_{\mathrm{open},2}$ the solution for an open elbow is calculated. Figure 7 shows the pressure distribution over time and space.

The same pattern as in figure 3 is given. There are three nodes, one at the beginning, one in the middle and one at the end of the elbow. Additionally, there is an anti-node in between two nodes respectively. A difference to the 1-D solver is the pressure distribution in the horizontal pipe, from $x = 0m$ to $x = 0.1m$, which is slightly warped in comparison to figure 3.

The second case is a semi closed sharp elbow. The excitation frequency is the second harmonic frequency $f_{2,closed}$ for a semi closed pipe. The expected pressure distribution is calculated by the 2-D solver (figure 8). The characteristic number of nodes and antinodes for a semi closed pipes can be seen. Two nodes, one at the beginning and one at two thirds of the elbow's total length and two antinodes, one at one third and one at the end can be observed. Obviously the difference between the 2-D solver of a sharp edged elbow and 1-D solver is negligible which would not justify the computational effort for the acoustic case. In the following chapter another numerical test is presented

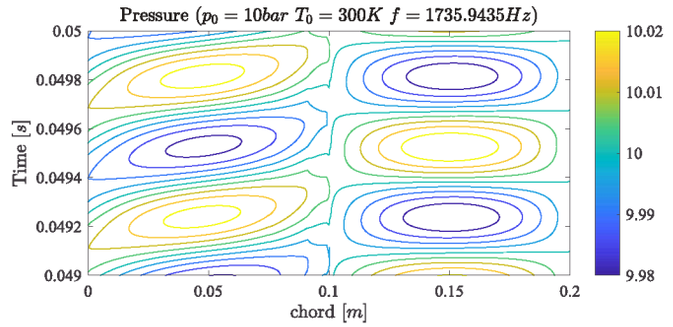

Figure 7: Open end elbow resonator test

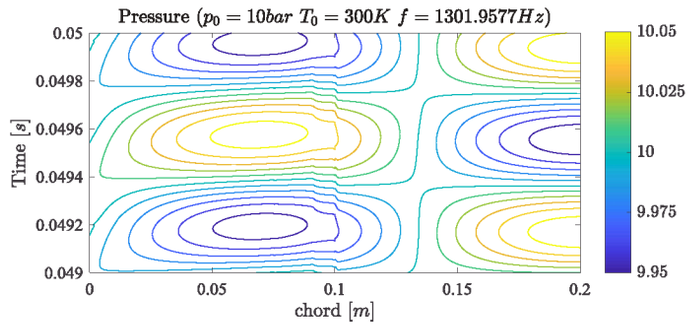

Figure 8: Closed end elbow resonator test

4 Closed shock tube test case

The shock tube is a classical test case for numerical Riemann solvers to examine its performance for discontinuities /6/, /7/. A pipe with an isothermal gas has an initial pressure and density discontinuity distribution in the middle. This initial set up allows to produce shock waves of arbitrary strength by increasing of the initial pressure difference resulting a higher amplitude of the shock wave and in a faster traveling speed which is always supersonic. It can be expected that in contrast to the acoustic waves which are of negligible altitude and

which travel with the speed of sound the reflexion of shock waves will be stronger within the sharp edge region of an elbow. Hence, the results for the two dimensional solver are expected to be different compared to the 1-D solution and reproduce the physics more exactly. To validate the results of the 2-D solver, a 3-D CFD simulation of the elbow is used.

4.1 Closed shock tube

To understand the effects of shockwave reflection in a sharp elbow, a numerical shock tube experiment in a closed straight pipe using the 1-D solver is presented. A pipe with a length of $L = 0.2m$, an initial temperature $T_0 = 300\,K$, the left region with high pressure $p_{high} = 16bar$ and the right region with low pressure $p_{low} = 1bar$ is considered. Figure 9 shows the pressure distribution at four different time steps. The initial distribution (blue line) causes a rarefaction wave travelling to the left and a shockwave travelling to the right (red line). As soon as the shockwave hits the wall it is reflected and moving to the left (black line). The same phenomenon occurs when the shockwave hits the left wall. At $t = 0.088061ms$ (green line) the rarefaction wave has been reflected, travelling to the right and interacts with the shockwave.

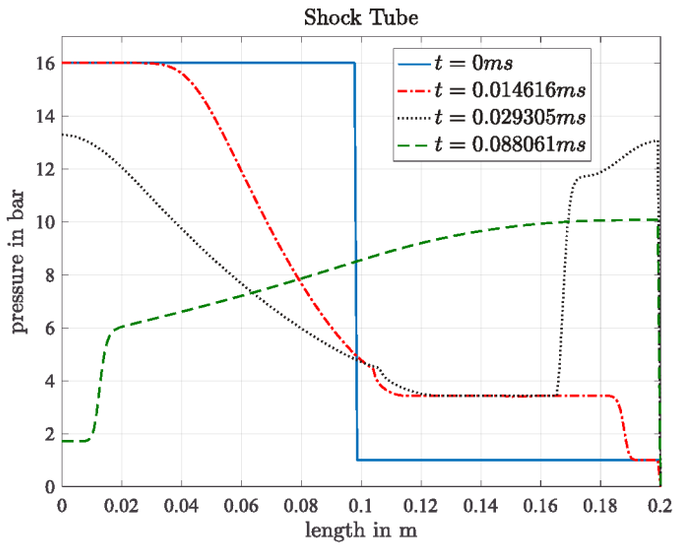

Figure 9: Pressure distribution of a closed Shock Tube.

4.2 Closed shock elbow

Now, a numerical shock tube experiment for an elbow with a total length of 0.1 m is presented, figure 10 depicts its initial conditions. The virtual membrane separating high and low pressure regions is located at $x = 0.03m$. The high pressure region is on the left side and the low pressure region on the right side of a membrane. As depicted in figure 10 the pressure at the three following locations is recorded: $x = 0.0099\,m$, $x = 0.04\,m$, $y = 0.02\,m$. The 3-D CFD simulation has been calculated with the solver FLUENT 17 using an explicit solver and applying the k-epsilon model.

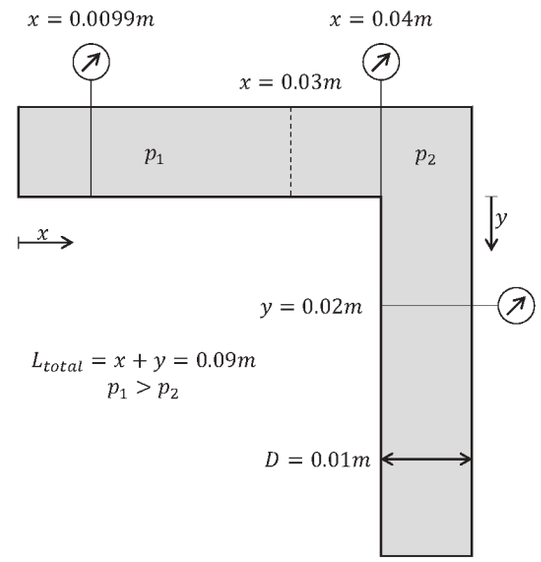

Figure 10: Shock tube experiment in an elbow.

The solution of the two dimensional solver simulation of the elbow is represented by the black curve and a 1-D simulation of a pipe is represented by the red curve (figure 11). Both curves are drawn in comparison to the green curve which shows the distribution of the CFD simulation.

Firstly, the pressure at the virtual sensor at $x = 0.0399m$ is analysed because the effect of a partial shock reflection is strongly apparent here. The incoming shock wave causes a discontinuous pressure jump at 0,001 ms. The pressure remains constant until 0,01ms for the 2-D solver and the CFD simulation starts to rise, whereas the 1-D pressure remains constant. In comparison to the 1-D shock tube (cf. figure 9) it can be seen that the reflected shockwave causes another pressure rise. That corresponds to the pressure rise at 0.01ms in the CFD and the 2-D calculation, which results from the partially reflected shockwave at the right wall of the elbow.

The steady decrease of pressure from 0.013 ms until 0.027 ms also corresponds qualitatively to the 1-D solution, but the pressure amplitude is higher due to the partial reflection at the right wall of the elbow. At 0.027 ms the pressure starts to rise again which is caused by the arriving shockwave which was reflected by the wall at the bottom of the elbow. Since the initial shock wave travelled through the sharp elbow geometry it was sheared, that is why the pressure rise is not discontinuous but steady. Remarkably, at 0.03 ms the pressure for the 1-D pipe reaches the same level as both the 2-D and the 3-D CFD elbow. From 0.031ms all three pressure distributions equals each other until 0.052 ms. Here, the two pressure peaks occurring at 0,053 ms and 0,059 ms result from the returning two shock waves which were produced by the subdivision of the initial shock hitting the sharp elbow geometry.

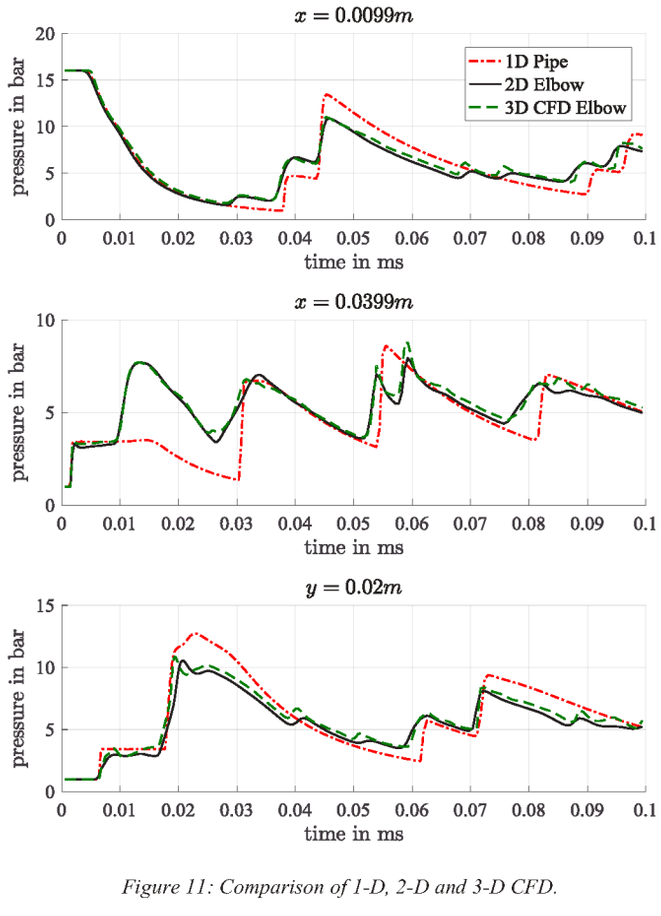

Figure 11: Comparison of 1-D, 2-D and 3-D CFD.

The other two pressure sensors show the same pattern. All three solutions follow each other right until the partially reflected shockwave reaches the pressure sensors in contrast to the 1-D solution. That can be seen in the pressure distribution of the sensor at $x = 0.009m$. The pressure is constant until the rarefaction wave provokes a steady decrease of pressure. At 0.03 ms the 1-D solution deviates from the 2-D and 3-D solution. The reason for this, is that the 1-D solver cannot calculate a partial reflection caused by an elbow. A pressure jump in the 1-D pressure is only provoked by the main shockwave reflecting at each closed pipe end.

That is not the case for the 2-D and 3-D pressure distribution. While the first partially reflected shockwave is swallowed by the rarefaction wave, the second partially reflected shockwave at the left wall causes a pressure rise at 0.03 ms. Both following pressure jumps are provoked by the main shockwave travelling first to the left wall (0.038 ms) and subsequently reflecting to the right again (0.044 ms). These two correspond to the 1-D solution. With progressive time the pressure jumps caused by the shockwaves repeat themselves.

The repetition of the shockwaves can also be seen on the basis of the pressure distribution of the third sensor at $y = 0.02\,m$. At 0.006 ms the main shockwaves reaches the sensor and returns at 0.018 ms. Until that point all three solutions are equal, but at 0.02 ms a partially reflected shockwave on the upper wall of the elbow occur. After two more pressure jumps caused by various partially shockwaves the main shockwave causes two pressure rises at 0.06 ms and 0.07 ms.

The 2-D simulation of the elbow follows CFD simulation sufficiently. Every increase and decrease in pressure is represented by the 2-D solver. The one dimensional solution has a larger deviation than the 2-D solution, especially near the sharp edge at $x = 0.0399\,m$. Table 1 summarises the mean deviation over time for each virtual pressure sensor. The two dimensional solver assures a deviation lower than 7 %, whereas the deviation of the 1-D model is between 12% and 29% and is therefore inacceptable compared to the 2-D solver solution.

Pressure Sensor Position	*1D*	*2D*
$x = 0.009m$	12,4%	6,93%
$x = 0.0399m$	28,8%	3,11%
$y = 0.02m$	12,88%	7,16%

Table 1: Mean pressure deviation in reference to CFD

5 Summary and Conclusion

This paper presents an approach to modulate a sharp edged elbow using a coupling of a two dimensional and a one dimensional finite volume solver. The approach is validated in two ways: For small pressure disturbances analytical solution from the acoustic theory is compared to the solver's solution and for large pressure disturbances Sod's Shock Tube experiment for a closed pipe is examined. It has been revealed that for the acoustic case, i.e. for a small disturbance there is barely a difference the approaches and therefore the computational effort is not justified. But for large disturbances the one dimensional solver reveals an inacceptable deviation and it is necessary to apply the two dimensional approach if shock phenomena are expected. Since the computational time of the two dimensional solver is in the order of several minutes, whereas the CFD calculation presented above took 35 hours the two dimensional approach is to be preferred. Although for the shown case the deviation of the two dimensional solver is rather acceptable compared to the one dimensional approach, there is still improvement potential for future works which can be summarised in two main tasks. The given solver does not include friction and the flow is assumed to be planar which implies that the solver does not take dissipation into account and the curvature of the streamline caused by the sharp edge at the area where the upper and lower pipe hit each other is neglected. Both phenomena can be treated introducing a source term and will be subject to future works.

Nomenclature

Variable	*Description*	*Unit*
a	Speed of sound	$\left[\frac{\mathrm{m}}{\mathrm{s}}\right]$
c_v	Isochoric heat capacity	$\left[\frac{\mathrm{J}}{\mathrm{kg} * \mathrm{K}}\right]$
e	Specific Energy	$\left[\frac{\mathrm{J}}{\mathrm{m}^3}\right]$
f	Frequency	$\left[\frac{1}{\mathrm{s}}\right]$
F	Horizontal Flux	$[-]$
G	Vertical Flux	$[-]$
I	Momentum	$\left[\frac{kg * m}{s}\right]$
L	Length	$[m]$

M	Mass	$[kg]$
p	Pressure	$\left[\frac{N}{m^2}\right]$
R	Gas constant	$\left[\frac{J}{kg * K}\right]$
T	Temperature	$[K]$
t	Time	$[s]$
U	Conservative variables	$[-]$
u	Horizontal velocity	$\left[\frac{m}{s}\right]$
v	Vertical velocity	$\left[\frac{m}{s}\right]$
W	Width	$[m]$
x	Horizontal coordinate	$[-]$
y	Vertical coordinate	$[-]$
κ	Heat capacity ratio	$[-]$
λ	Eigenvalue in x-direction	$\left[\frac{m}{s}\right]$
ρ	Density	$\left[\frac{kg}{m^3}\right]$
ξ	Eigenvalue in y-direction	$\left[\frac{m}{s}\right]$

References

/1/ Steger, J. L., Warming F. R., "*Flux Vector Splitting of the Inviscid Gasdynamic Equations with Application to Finite-Difference Methods*", Journal of Computational Physics 40, pp. 263-293, 1981.

/2/ Toro, E. F., "*Riemann Solvers and Numerical Methods for Fluid Dynamics*", Springer Verlag, 2009.

/3/ Hirsch, C. "*Numerical Computation of Internal and External Flows*", Elsevier, 2007.

/4/ Möser, M., "*Technische Akustik*", p.42, Springer Verlag, 2015.

/5/ Kinsler, L. E., "*Fundamentals of Acoustics*", p. 202, Wiley, 1962.

/6/ Sod, G. A., *A Survey of Several Finite Difference Methods for Systems of Nonlinear Hyperbolic Conservation Laws*, Journal of Computational Physiks 27, p. 1-31, 1978.

/7/ Lora-Claijo, F.D. et al., *Exact solution of the 1D Riemann problem in Newtonian and relativistic hydrodynamics*, Revista Mexicana de Fisica E 59, p. 28-50, 2013.